WARSAW UNIVERSITY OF TECHNOLOGY Index 351733
FACULTY OF CIVIL ENGINEERING
COMMITTEE FOR CIVIL AND WATER ENGINEERING
POLISH ACADEMY OF SCIENCES ISSN 1230-2945

DOI: 10.24425/ace.2026.1415

ARCHIVES OF CIVIL ENGINEERING

Vol. LXXII ISSUE 3 2026



pp. 555 –569



**Research paper**

# Vehicle-bridge coupled dynamic response of cable-stayed bridges under heavy-cargo transportation loads

**Zhigao Long[1], Che Yao[2]**

**Abstract:** The burgeoning market for heavy-cargo transportation poses an increasing challenge to the normal use of highway bridges. This study investigates the vehicle-bridge coupled dynamic response of a twin-tower three-span cable-stayed bridge under the load of heavy-cargo transportation by employing the holistic solution method and the direct integration method. The influence of vehicle load and speed on the dynamic response of the bridge when heavy-cargo transportation vehicles pass through cable-stayed bridges is discussed. The main research conclusions are: (1) The peak stress of the stay cables increases linearly with the increase in load weight. There is a nonlinear relationship between the vibration amplitude of the stay cables and the vehicle load parameters, with the rate of increase in the vibration amplitude accelerating as the load weight increases. (2) The maximum displacement values of the towers show a trend of linear increase with the load parameters. The deflection at the mid-span cross-section increases linearly with the load weight, with an increase of approximately 26.8 mm in mid-span deflection for every additional 100t of load weight. (3) The vehicle speed has a significant influence on the cable vibration amplitude, with the growth rate of the vibration amplitude continuously increasing as the vehicle speed increases. (4) The displacement of two bridge towers shows a positive correlation with vehicle speed variation. The oscillation amplitude of the displacement at the mid-span cross-section shows a clear increase.

**Keywords:** cable-stayed bridge, heavy-cargo transportation, vehicle-bridge coupled vibration, dynamic response

[1]BSc., Eng., Department of Bridge Engineering, School of Civil Engineering, Central South University, Changsha, Hunan, 410075, China, e-mail: Longzhigao_2024@163.com, ORCID: 0009-0004-4469-3205
[2]MSc., Eng., Department of Bridge Engineering, School of Civil Engineering, Central South University, Changsha, Hunan, 410075, China, e-mail: wtcybq@126.com, ORCID: 0009-0000-9237-4197

# 1. Introduction

With the continuous development of the global economy, the demand for high added-value, non-dismountable large objects remains, and the heavy-cargo transportation industry will continue to thrive [1]. Along the heavy-cargo transportation routes, there are usually numerous bridges with varying technical conditions. When heavy-cargo vehicles pass over bridges, the phenomenon of vehicle-bridge coupled vibration is very pronounced. Especially for long-span bridges, there are noticeable differences in the components under static loads and vehicle loads [1–3].

Building upon classical models, modern vehicle-bridge coupling models have introduced more accurate vehicle models and employed finite element methods to discretize bridges [4–6]. Li conducted a study on the dynamic response and impact factors of cable-stayed bridges under vehicle- bridge coupling effects using finite element modeling [7]. Li investigated the impact effects on the main beam, bearings, cable-stayed tendons, and bridge towers of a long-span railway cable-stayed bridge at various vehicle speeds [8]. Zhu et al. assessed the driving safety of vehicles on coastal cable-stayed bridges and the safety of the bridges themselves [9]. Song utilized the orthogonal relationship of the precise modal shapes of a linearized undamped cable-stayed bridge model and transformed the original nonlinear coupled partial differential equations of the cable-stayed bridge model into a set of ordinary differential equations using the Galerkin method [10]. Additionally, numerous numerical computation methods have been proposed by scholars for solving coupled vibration equations [11–13].

Therefore, this study investigates the vehicle-bridge coupled dynamic response of a twin-tower three-span cable-stayed bridge under heavy-cargo transportation, explores the dynamic response of the bridge under special loads and its influencing factors, and lays the foundation for subsequent research on the safety and durability of bridge structures.

# 2. Model establishment

## 2.1. Cable-stayed bridge model

This study takes the Ganxigou Bridge in Eastern Chongqing as the research subject, as shown in Fig. 1. The main bridge has a span of 670 meters, with a span combination of 155+360+155 meters, and is a double-tower, three-span, double-cable-plane concrete cable-stayed bridge with a fully floating structural system and a self-anchored anchorage method. The main towers are designed in a gem-shaped concrete hollow column form, with Tower 1 at a height of 147 meters and Tower 2 at a height of 182 meters. The bridge deck is 27.1 meters wide, with a main beam height of 2.5 meters, and a transverse diaphragm is set every 8 meters. There are 22 cables symmetrically arranged on each side of the central span and side span, totaling 90 cables.

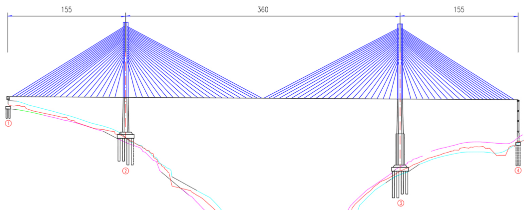


Fig. 1. Layout of Ganxigou Bridge

This study utilizes ABAQUS for modeling the studied bridge. In the finite element model of the bridge, the bottom of two towers and two ends of the main beam are fixed with 6 DOFs. The main towers are modeled using B31 spatial linear beam elements, the stay cables are modeled using T3D2 spatial linear truss elements, and the main beams and cross-diaphragms are modeled using C3D8R eight-node linear hexahedral elements with reduced integration for internal interpolation calculations within the elements. The established finite element model is shown in Fig. 2. Utilizing ABAQUS, modal analysis calculations are performed on the bridge to determine the first five vibration modes and frequencies, as shown in Fig. 3.

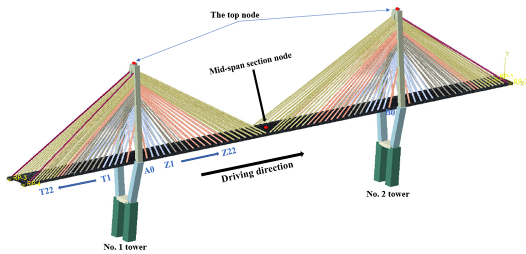


Fig. 2. Finite element model of Ganxigou Cable-Stayed Bridge

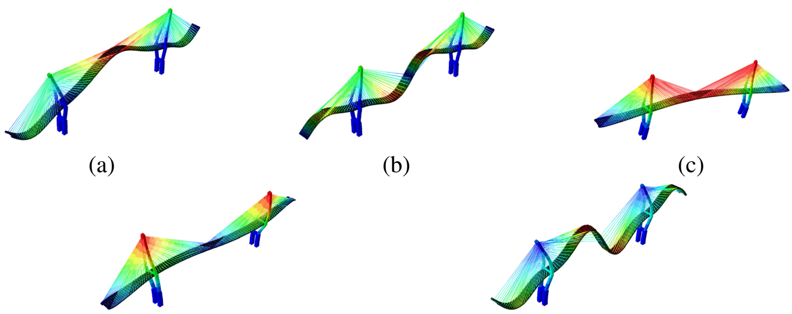

(a) (b) (c)

(d) (e)

Fig. 3. Illustrations of the first five vibration modes; (a) First mode ($f$ = 0.285 Hz), (b) Second mode ($f$ = 0.316 Hz), (c) Third mode ($f$ = 0.0.323 Hz), (d) Fourth mode ($f$ = 0.387 Hz), (e) Fifth mode ($f$ = 0.511 Hz)

## 2.2. Vehicle model

This study takes the 14-axle hydraulic flatbed trailer produced by Wanshan Company as the research subject. The vehicle is composed of one 2-axle, two 3-axle, and one 6-axle modular unit trucks, with an axle track of 1.6 meters and a lateral wheel track of 2.28 meters. A schematic diagram of the vehicle is shown in Fig. 4.

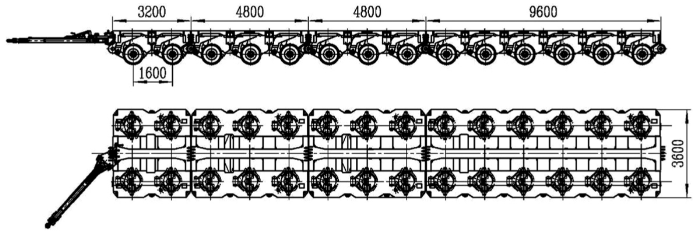


Fig. 4. 14-axle hydraulic combination semi-trailer (Unit: cm)

The vehicle studied in this paper is simulated using the ABAQUS finite element software. The vehicle body is modeled using C3D8R solid elements, and the elastic damping characteristics of the suspension and wheels are simulated using two-point connected spring-damper units. The specific parameters of the vehicle are shown in Table 1.

Table 1. Hydraulic flatbed semi-trailer vehicle parameters

| Parameters | Values | Parameters | Values |
|---|---|---|---|
| Rated load capacity (kg) | 500000 | Vehicle body pitch moment of inertia ($kg{\cdot}m^2$) | 127982 |
| Maximum total vehicle weight (kg) | 560000 | Vehicle body roll moment of inertia ($kg{\cdot}m^2$) | 23200000 |
| Wheel weight (m) | 670 | First-stage spring stiffness ($N{\cdot}m^{-1}$) | 2400000 |
| External dimensions (m) | 22.4×3.6×1.32 | First-stage spring damping($N{\cdot}s{\cdot}m^{-1}$) | 25000 |
| Axle spacing (m) | 1.6 | Second-stage spring stiffness ($N{\cdot}m^{-1}$) | 4400000 |

Taking the bridge length $L = 670$ m and calculating the road step length $\Delta L = 0.5\ m$, the number of simulation calculations for the bridge road surface irregularity is N. Based on the road power spectrum suggested by the Chinese standard (GB/T7031-2005) [14] for simulating bridge surface irregularity, we consider road surfaces of grade C, with the geometric mean for $m \lg \Delta\sigma + \lg \mathrm{N} = \lg \mathrm{C}$ taken as 256. Using Visual Studio 2017 with C++, a program is written to calculate the road surface irregularity time series samples, and the resulting curves are shown in Fig. 5. This study employs the holistic solution method to establish the vehicle-bridge coupled vibration equations. Compared with the non-iterative partitioned method with energy conservation properties proposed in [15], the immediate integration method adopted in this study maybe more accurate.

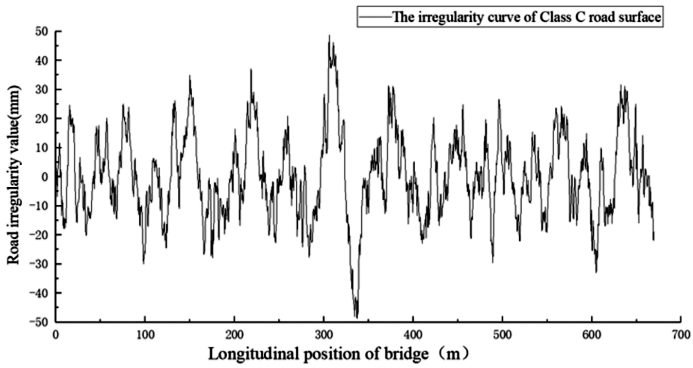


Fig. 5. Level C roughness sample curves

# 3. Results analysis

## 3.1. The influence of total vehicle weight

This section discusses the impact of vehicle load weight on the dynamic response of the heavy-cargo vehicle-bridge coupling system. It considers the following four scenarios for the heavy-cargo vehicle traveling at a constant speed ($V = 5$ m/s) on a road surface with level C irregularity, moving in one direction and centrally located on the bridge: total vehicle and cargo weight of 200 t (axle load of 14.3 t), 300 t (axle load of 21.4 t), 400 t (axle load of 28.6 t), and 500 t (axle load of 35.7 t). The initial vehicle weight is set to $m_0 = 200$ t, and the load parameter $t = m/m_0$ is defined to discuss the changes in bridge dynamic response when $t = 1, 1.5, 2$, and 2.5.

### 3.1.1. Dynamic response of cables

Figure 6(a) illustrates the stress variation curve of cable $T_{22}$ under different total vehicle weights. It can be observed that cable $T_{22}$ experiences two stress extrema (minimum point A and maximum point B), and the stress variation at both extrema increases with the increase in load weight. The stress variation at the minimum point A grows linearly with the increase in load, with an increase of approximately 6.5 MPa for every additional 100 t of load. Figure 6(b) illustrates the stress variation curve of cable $Z_{22}$ under different load parameters. It can be seen that cable $Z_{22}$ experiences three stress extrema (minimum point B and maximum points A and C).

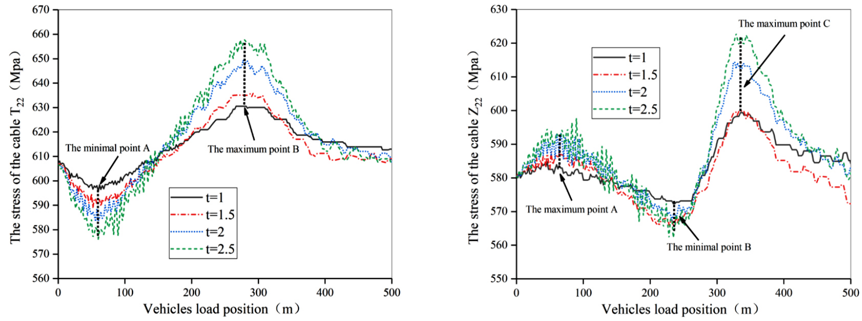


(a) (b)

Fig. 6. Stay cable stress variations under different load weights: (a) Cable $T_{22}$; (b) Cable $Z_{22}$

As shown in Fig. 7(a), the stress variation of cable $T_{22}$ is relatively large under different load conditions, with the maximum stress variation reaching 50.7 MPa when $t = 2.5$. Cable $Z_{22}$ has a smaller stress variation than cable $T_{22}$ at maximum point A and minimum point B, but there is a noticeable amplification at maximum point C. When $t = 2$ and $t = 2.5$, the stress increase is very pronounced, with the stress increment increasing by 81.2% and 125.6% compared to when $t = 1$. Figure 7(b) represents that due to the increase in load weight, the amplitude of the cable vibration exhibits nonlinear growth, and the stress peak values also increase accordingly.

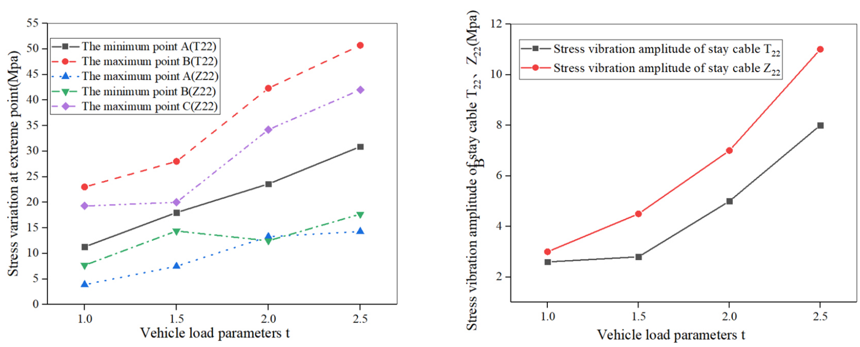


(a) (b)

Fig. 7. Parameter variation versus load weight variation: (a) Cable stress; (b) Cable vibration amplitude

The stress variation of cable $T_{11}$ under different load parameters are shown in Fig. 8. As shown in Fig. 8, the dynamic response of cable $T_{11}$ closely matches the results of the static calculation, indicating that the stress peak at the extreme point A increases approximately linearly with load. There is a significant difference between the dynamic response and static calculation results at the maximum point C of the cable.

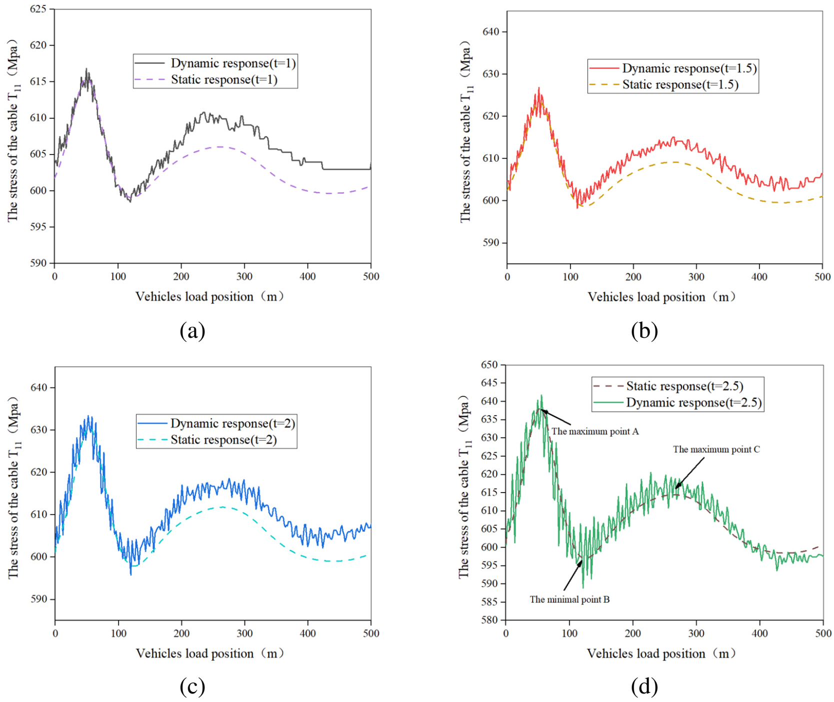


Fig. 8. Stress variation of cable $T_{11}$: (a) $t = 1$; (b) $t = 1.5$; (c) $t = 2$; (d) $t = 2.5$

Figure 9(b) illustrates that as the load increases, the rate of change of the cable stress vibration amplitude increases, leading to more intense stress oscillations.

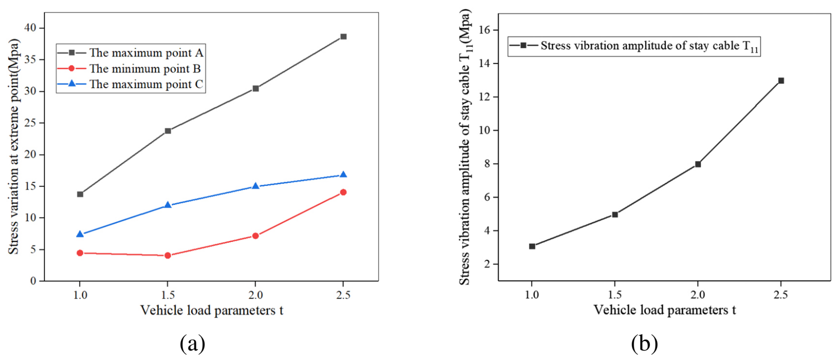


Fig. 9. Parameter variation of Cable $T_{11}$ versus load weight variation: (a) Cable stress; (b) Cable vibration amplitude

The stress variation curves of cable $T_0$ under different load parameters are shown in Fig. 10. As shown in Fig. 10, the dynamic stress response curve of cable $T_0$ closely matches the static results, indicating that the stress peak of cable $T_0$ tends to increase linearly with the increase in load. Within the first 100 meters of vehicle travel, changes in load have a noticeable impact on the stress oscillation amplitude of cable $T_0$.

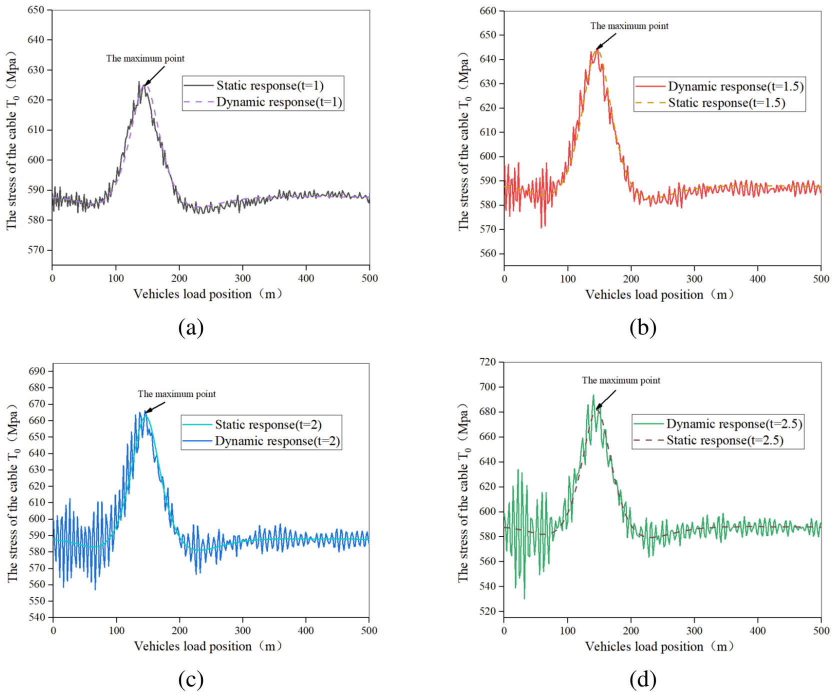


Fig. 10. Stress variation of cable $T_0$: (a) $t = 1$; (b) $t = 1.5$; (c) $t = 2$; (d) $t = 2.5$

The maximum stress amplitude varies with the load parameter, as shown in Fig. 11. This indicates that the stress amplitude of cable $T_0$ is highly sensitive to load factors, and the stress oscillation amplitude exhibits a nonlinear increase with increasing load.

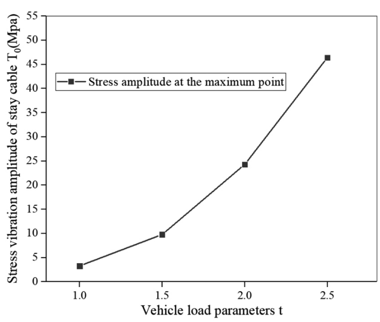


Fig. 11. Maximum vibration amplitude of cable $T_0$ stress – load variation

### 3.1.2. Dynamic response of bridge tower displacement

Figure 12 illustrate the longitudinal displacement variation curves of Tower 1 and Tower 2 under different load parameters. It can be observed from the figures that as the heavy vehicle passes over the bridge, both bridge towers exhibit a bivariate "S" shaped displacement change with double extrema. By plotting the displacement extrema versus load parameter graphs (Fig. 13), it is evident that the maximum displacement of both towers increases linearly with the load parameter, and the minimum displacement of the towers decreases with the increase in load, which can be approximated as a linear change.

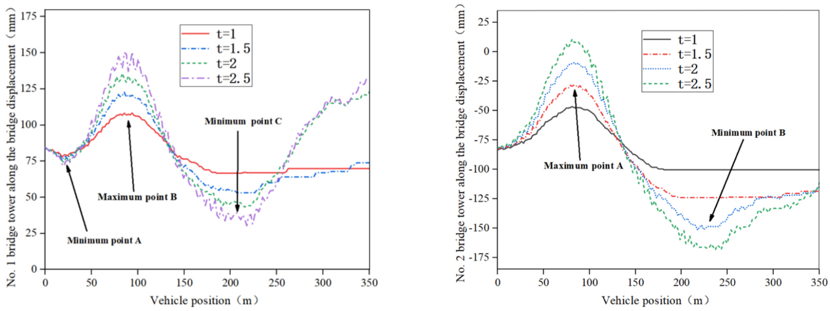


(a) (b)

Fig. 12. Longitudinal displacement variation curves of the bridge towers: (a) Tower 1; (b) Tower 2

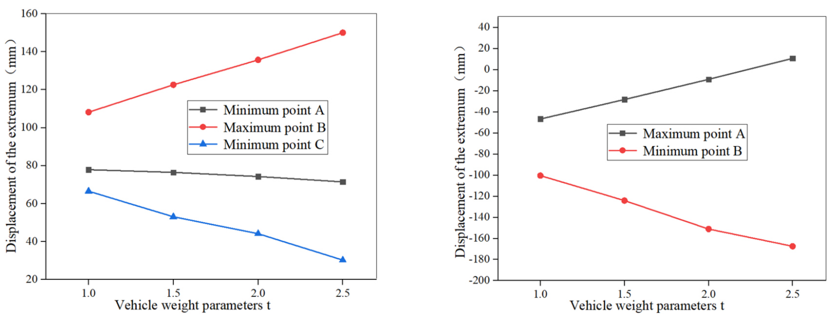


(a) (b)

Fig. 13. Displacement variation versus load variation: (a) Tower 1; (b) Tower 2

### 3.1.3. Dynamic response of the mid-span cross-section

Figure 14 presents the vertical displacement variation curve for the mid-span cross-section. The maximum deflection at the mid-span cross-section (absolute value of displacement at point B) increases linearly with the increase in load weight, with an increase of approximately 26.8 mm in mid-span deflection for every additional 100 t of load. After the vehicle enters the bridge and before it leaves, the mid-span cross-section moves upward, exhibiting displacement maximum points A and C. The displacement at these points, as shown in Fig. 15, decreases in slope with the change in load, indicating a downward trend in the rate of change with respect to load variation.

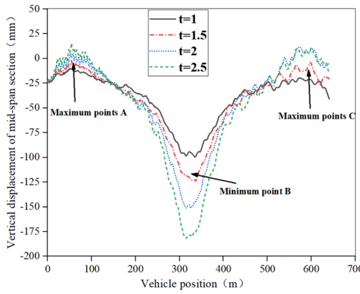


Fig. 14. Mid-span cross-section vertical displacement versus load parameter variation

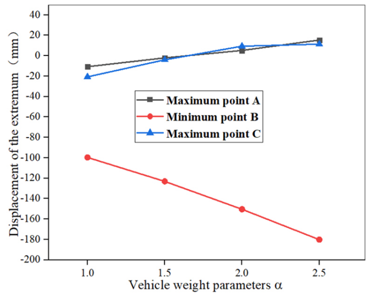


Fig. 15. Variation in mid-span cross-section displacement versus load parameter variation

## 3.2. The impact of vehicle speed

This section discusses the impact of vehicle speed on the dynamic response of the heavy-cargo vehicle-bridge coupling system [16], studying the dynamic response of the bridge under various vehicle speed scenarios. The heavy-cargo vehicle travels in one direction and is centrally located, with a vehicle load of 400 t (axle load of 28.57 t) and a road surface grade of C. The initial vehicle travel speed is $V_0$ = 2.5 m/s. The travel speeds of heavy-cargo vehicles are normally limited below 10m/s by relevant administration departments to avoid large vibration of the bridge. Therefore, the speed parameter $\alpha = V/V_0$ is defined to discuss the changes in bridge dynamic response when $\alpha$ ranges from 1 to 4.

### 3.2.1. Dynamic response of cables

Figure 16 illustrate the stress-time curves of cables $T_{22}$ and $Z_{22}$ under different speed parameters. By plotting the variation of peak stresses in the stress-time history against the speed parameter (as shown in Fig. 17(a)), it is observed that the peak stress of the stay cables does not change significantly with speed. However, the stress vibration amplitude of the stay cables is significantly affected by the speed, as shown in Fig. 17(b), where the stress increment of cable $Z_{22}$ is greater than that of cable $T_{22}$.

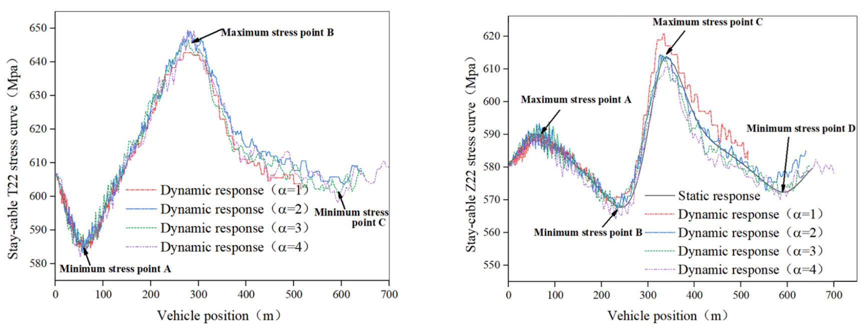


(a) (b)

Fig. 16. Stay cable stress variations under different speeds: (a) Cable $T_{22}$; (b) Cable $Z_{22}$

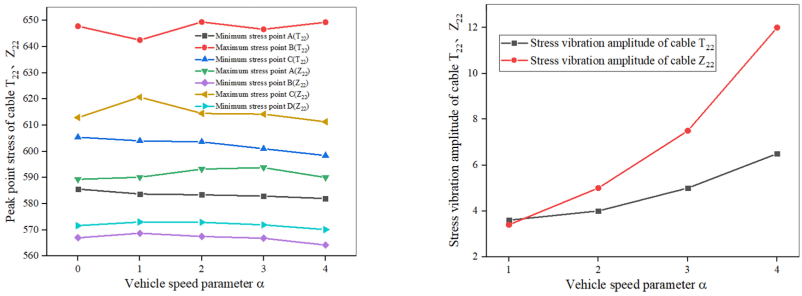


(a) (b)

Fig. 17. Parameter variation versus speed variation: (a) Cable stress; (b) Cable vibration amplitude

Figure 18 illustrate the stress variation curves of cable $T_{11}$ under different speed parameters. Comparing the dynamic and static stress changes, it can be observed that before the stress minimum point B, the vibration amplitude of cable stress increases with the increase in speed, and the stress path generally matches the static response results. After point B, the stress variation curve of cable $T_{11}$ deviates from the static calculation results. Figure 19(a) shows the stress variation at the extremum points with respect to the speed parameter. The stress at the minimum point A is nearly linearly related to speed changes, while the stress variation at points B and C continues to increase. Figure 19(b) indicates that the stress vibration amplitude of cable $T_{11}$ exhibits nonlinear growth with increasing speed.

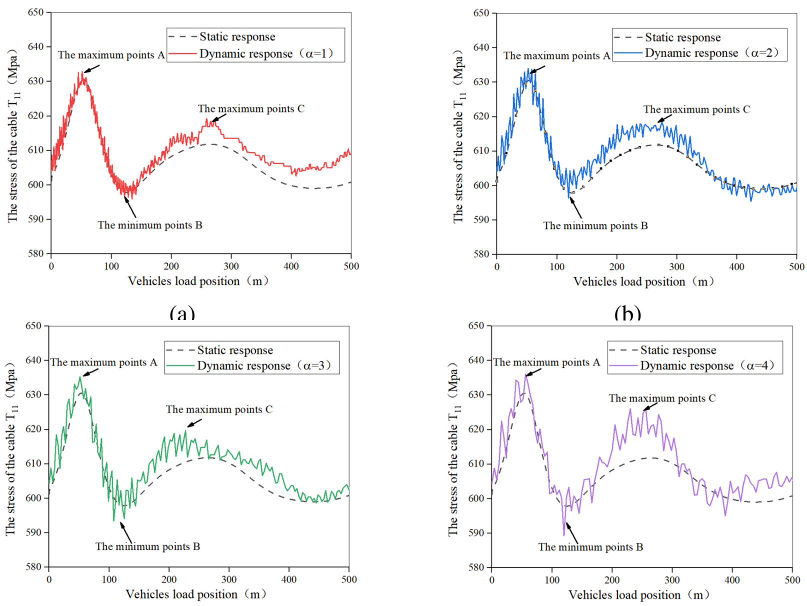


(a) (b) (c) (d)

Fig. 18. Stress variation of cable $T_{11}$: (a) $\alpha = 1$; (b) $\alpha = 2$; (c) $\alpha = 3$; (d) $\alpha = 4$

Figure 20 present the stress variation curves of cable $T_0$ under different speed parameters. The dynamic response curve of $T_0$ cable stress closely matches the static response results. The increase in the peak stress is primarily due to the increase in the stress vibration amplitude of the cable, with peak stresses being 661.3 MPa ($\alpha = 1$) and 673.8 MPa ($\alpha = 4$). Within the first 100 meters of vehicle travel, the cable stress vibrates intensely, and the stress vibration amplitude increases with increasing speed. The variation curves of the stress vibration amplitude and peak stress of cable $T_0$ with speed are shown in Fig. 21, and the growth trends of both curves are essentially the same.

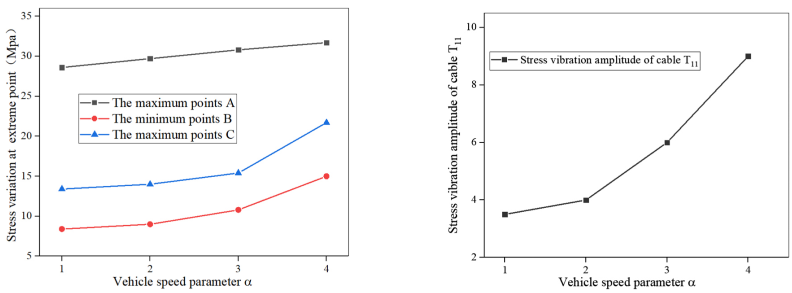


(a) (b)

Fig. 19. Parameter variation of Cable $T_{11}$ versus speed variation: (a) Cable stress; (b) Cable vibration amplitude

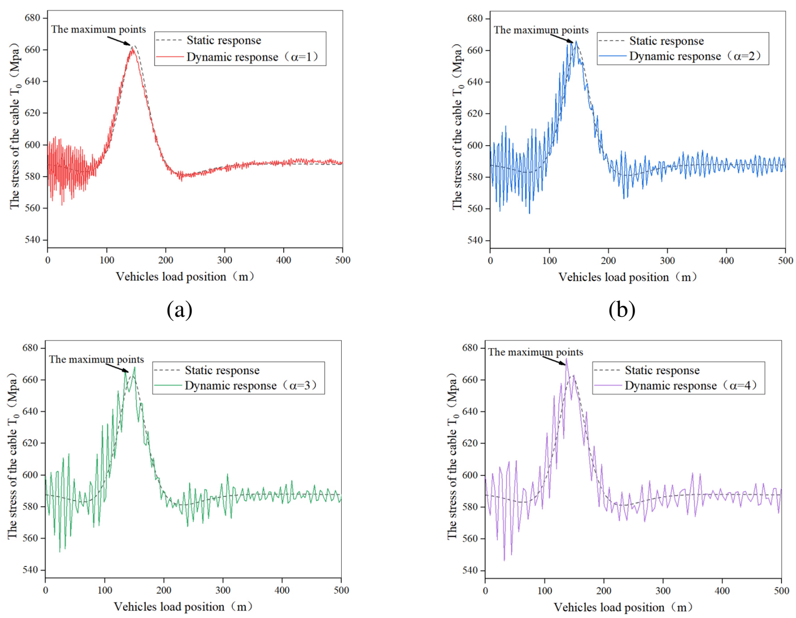


(a) (b) (c) (d)

Fig. 20. Stress variation of cable $T_0$: (a) $\alpha = 1$; (b) $\alpha = 2$; (c) $\alpha = 3$; (d) $\alpha = 4$

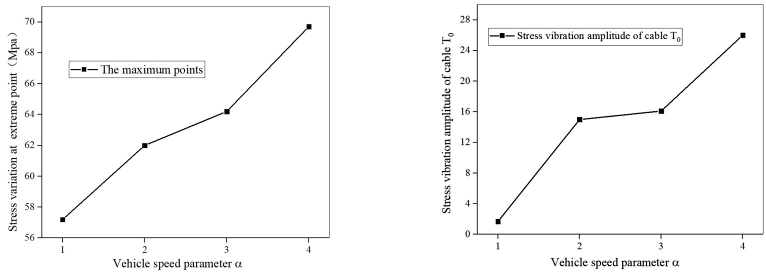


(a) (b)

Fig. 21. Parameter variation of Cable $T_0$ versus speed variation: (a) Cable stress; (b) Cable vibration amplitude

### 3.2.2. Dynamic response of bridge tower displacement

As shown in Figs. 22 and 23, comparing the displacement curves of Tower 1 and Tower 2, it is found that the abscissas of the displacement extremum points of both towers significantly shift backward with the increase of the speed parameter, indicating that an increase in speed delays the occurrence of peak displacement of the bridge towers. When the vehicle travels to the mid-span, the towers deflect towards the mid-span side, followed by a displacement minimum point. When $\alpha \geq 2$, the rate of displacement changes at the extremum points C of Tower 1 and B of Tower 2 increases, which is reflected as a noticeable increase in the slope of the curves in Fig. 23.

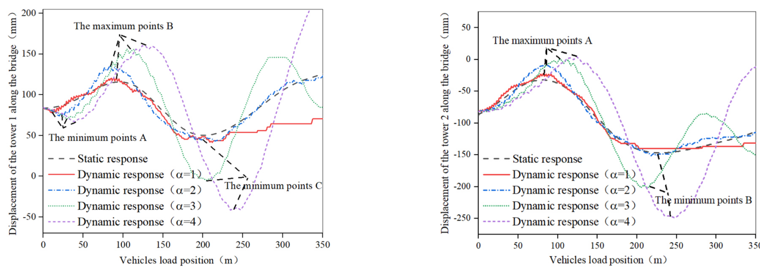


(a) (b)

Fig. 22. Longitudinal displacement variation curves of the bridge towers: (a) Tower 1; (b) Tower 2

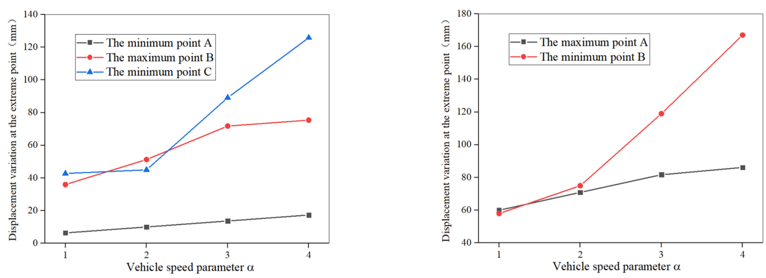


(a) (b)

Fig. 23. Displacement variation versus speed variation: (a) Tower 1; (b) Tower 2

# 4. Conclusions

1. The peak stress of the stay cables increases linearly with the increase in load weight; when the load weight exceeds this range (either too large or too small), the stress in the stay cables exhibits a distinct nonlinear behavior. The vibration amplitude of cable T0 is most affected by the load parameters compared to others.
2. The displacement of both bridge towers exhibits a bivariate "S" shaped displacement change with double extrema, and the maximum displacement values of the towers show a trend of linear increase with the load parameters.
3. The vehicle speed has a minimal impact on the peak stress of stay cables but a significant influence on the cable vibration amplitude, with the growth rate of the vibration amplitude continuously increasing as the vehicle speed increases.
4. The displacement of two bridge towers shows a positive correlation with vehicle speed variation. The displacement peak at the second stress extremum point is significantly larger than that at the first extremum point, and when the speed exceeds 5 m/s, the displacement increases very rapidly with speed.

## References


[1] Y.S. Yang, Y.Q. Xiang, H. Lin, and Z.Y. Chen, "Study on vibration response of submerged floating tunnel considering vehicle eccentric load", *Applied Ocean Research*, vol. 110, art. no. 102598, 2021, doi: 10.1016/j.apor.2021.102598.

[2] K. Feng, A. González, and M. Casero, "A kNN algorithm for locating and quantifying stiffness loss in a bridge from the forced vibration due to a truck crossing at low speed", *Mechanical Systems and Signal Processing*, vol. 154, art. no. 107599, 2021, doi: 10.1016/j.ymssp.2020.107599.

[3] T. Nagayama, A.P. Reksowardojo, D. Su, and T. Mizutani, "Bridge natural frequency estimation by extracting the common vibration component from the responses of two vehicles", *Engineering Structures*, vol. 150, pp. 821–829, 2017, doi: 10.1016/j.engstruct.2017.07.040.

[4] X. Kong, D.J. Wu, C.S. Cai, and Y.Q. Liu, "New strategy of substructure method to model long-span hybrid cable-stayed bridges under vehicle-induced vibration", *Engineering Structures*, vol. 34, pp. 421–435, 2012, doi: 10.1016/j.engstruct.2011.10.018.

[5] Y. Huang, "Dynamic performance of bridge piers impacted by heavy trucks", *Archives of Civil Engineering*, vol. 69, no. 3, pp. 173–185, 2023, doi: 10.24425/ace.2023.146074.

[6] Y. Huang, "On the resistance of concrete hollow thin-walled high piers to rock collisions", *Archives of Civil Engineering*, vol. 69, no. 3, pp. 187–197, 2023, doi: 10.24425/ace.2023.146075.

[7] Z. Li, Z.D. Li, Y.S. Zhang, D.H. Chen, S.Z. Xu, and Y. Zhang, "Theoretical analysis and experimental study of vehicle-bridge coupled vibration for highway bridges", *Archive of Applied Mechanics*, vol. 94, no. 1, pp. 21–37, 2024, doi: 10.1007/s00419-023-02498-x.

[8] Y.L. Li, S.F. Dong, Y.L. Bao, K.J. Chen, and S.Z. Qiang, "Impact Coefficient Analysis of Long-Span Railway Cable-Stayed Bridge Based on Coupled Vehicle-Bridge Vibration", *Shock and Vibration*, vol. 2015, art. no. 641731, 2015, doi: 10.1155/2015/641731.

[9] J. Zhu, W. Zhang, and M.X. Wu, "Evaluation of Ride Comfort and Driving Safety for Moving Vehicles on Slender Coastal Bridges", *Journal of Vibration and Acoustics*, vol. 140, no. 5, art. no. 051012, 2018, doi: 10.1115/1.4039569.

[10] M.T. Song, D.Q. Cao, W.D. Zhu, and Q.S. Bi, "Dynamic response of a cable-stayed bridge subjected to a moving vehicle load", *Acta Mechanica*, vol. 227, no. 10, pp. 2925–2945, 2016, doi: 10.1007/s00707-016-1635-0.

[11] Y.B. Yang and C.W. Lin, "Vehicle-bridge interaction dynamics and potential applications", *Journal of Sound and Vibration*, vol. 284, no. 1-2, pp. 205–226, 2005, doi: 10.1016/j.jsv.2004.06.032.

[12] W.H. Guo and Y.L. Xu, "Fully computerized approach to study cable-stayed bridge-vehicle interaction", *Journal of Sound and Vibration*, vol. 248, no. 4, pp. 745–761, 2001, doi: 10.1006/jsvi.2001.3828.

[13] H.L. Yu, B. Wang, C.P. Xia, Z.Y. Gao, and Y.L. Li, "Efficient non-stationary random vibration analysis of vehicle-bridge system based on an improved explicit time-domain method", *Engineering Structures*, vol. 231, art. no. 111786, 2021, doi: 10.1016/j.engstruct.2020.111786.

[14] GB/T7031-2005 Mechanical vibration – Road surface profiles – Reporting of measured data. General Administration of Quality Supervision, Inspection and Quarantine of the PRC, 2005.

[15] P. Yuan, K.V. Yuen, M. Beer, C.S. Cai, and Y. Wan, "A non-iterative partitioned computational method with the energy conservation property for time-variant dynamic systems", *Mechanical Systems and Signal Processing*, vol. 209, art. no. 111105, 2024, doi: 10.1016/j.ymssp.2024.111105.

[16] X. Zheng, D.H. Yang, T.H. Yi, and H.N. Li, "Bridge influence line identification from structural dynamic responses induced by a high-speed vehicle", *Structural Control and Health Monitoring*, vol. 27, art. no. e2544, 2020, doi: 10.1002/stc.2544.

Received: 2024-12-20, Revised: 2025-02-04